Preserving large-scale features in simulations of elastic turbulence

Supplementary Material

Sumithra R. Yerasi[1], Jason R. Picardo[2], Anupam Gupta[3], and Dario Vincenzi[1]

[1]Université Côte d'Azur, CNRS, LJAD, 06100 Nice, France

[2]Department of Chemical Engineering, Indian Institute of Technology Bombay, Mumbai 400076, India

[3]Department of Physics, Indian Institute of Technology Hyderabad, Hyderabad 502284, India

1. Simulations with finite inertia

The main text examines different techniques for the numerical simulation of elastic turbulence in the Stokes limit. In particular, in § 3, two reformulations of the Oldroyd-B constitutive equation are compared, namely the Cholesky-log and the symmetric square root (SSR) decompositions. The corresponding simulations exhibit qualitatively different large-scale dynamics and flow structures. To identify the correct simulation, we make use of a mathematical bound for the determinant of the polymer conformation tensor $\boldsymbol{C}$ due to Hu & Lelièvre (2007): If $\det \boldsymbol{C}$ is initially greater than unity everywhere over the spatial domain, then it must continue to remain uniformly greater than unity at later times. We find that this bound is frequently violated by the SSR decomposition, whereas it is preserved by the Cholesky-log decomposition. We conclude that, for the same parameters and space-time resolution, the SSR decomposition is less accurate than the Cholesky-log decomposition and leads to erroneous large-scale dynamics.

In this supplementary section, we show that analogous conclusions hold when the motion of the solution is given by the Navier–Stokes equation rather than the Stokes equation. We consider the Oldroyd-B model (see § 2 of the main text for details):

$$\partial_t \boldsymbol{C} + \boldsymbol{u}\cdot\boldsymbol{\nabla}\boldsymbol{C} = \boldsymbol{C}\cdot\boldsymbol{\nabla}\boldsymbol{u} + (\boldsymbol{\nabla}\boldsymbol{u})^\top\cdot\boldsymbol{C} - \boldsymbol{T}_p, \tag{1.1a}$$

$$\partial_t \boldsymbol{u} + \boldsymbol{u}\cdot\boldsymbol{\nabla}\boldsymbol{u} = -\boldsymbol{\nabla} p + \nu\Delta\boldsymbol{u} + \nu_p\boldsymbol{\nabla}\cdot\boldsymbol{T}_p + \boldsymbol{F}, \tag{1.1b}$$

$$\boldsymbol{\nabla}\cdot\boldsymbol{u} = 0, \tag{1.1c}$$

where $\boldsymbol{T}_p = (\boldsymbol{C}-\boldsymbol{I})/\tau_p$. The setting and the numerical methods used to solve the above equations are the same as in the main text. The simulations are performed in the two-dimensional periodic square $V = [0, 2\pi]^2$ and the flow is driven by the cellular forcing $\boldsymbol{F}(x, y) = f_0(-\sin Ky, \sin Kx)$. For $\nu_p = 0$, the Newtonian solution $\boldsymbol{u} = -\boldsymbol{F}/\nu K^2$ is stable provided the associated Reynolds number $Re = U/\nu K$ (with $U = f_0/\nu K^2$) satisfies $Re < \sqrt{2}$ (Gotoh & Yamada 1984). We initialize the simulation with the Newtonian solution $\boldsymbol{u} = -\boldsymbol{F}/\nu K^2$ and the equilibrium polymer conformation $\boldsymbol{C} = \boldsymbol{I}$, and take $\nu = 0.05$, $f_0 = 0.02$, $K = 2$, $\tau_p = 50$, $\nu_p = 10^{-2}$. With this choice of parameters, the Reynolds number associated with the laminar solution is $Re = 1$; hence the Newtonian flow ($\nu_p = 0$) is stable, and the chaotic dynamics that we observe in the presence of polymers is solely due to elastic instabilities.

Fourth-order central differences are used to discretize the equations for the flow (in the vorticity-velocity formulation) and the polymer, except for the advection of the latter, which is treated according to the Kurganov & Tadmor (2000) scheme. The spatial resolution is 512^2. The time integration is based on a second-order Runge–Kutta scheme with a time step $\delta t = 8\times10^{-4}$.

Snapshots of $\mathrm{tr}\,\boldsymbol{C}$ from the Cholesky-log and the SSR simulations are compared in figure 1 (the

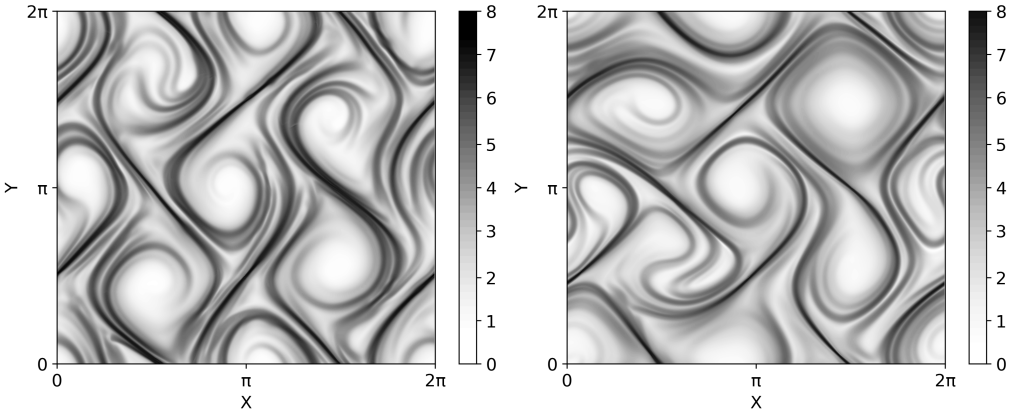

(*a*) (*b*)

FIG. 1: Representative snapshots (instantaneous) of the logarithm of tr $\boldsymbol{C}$ for (*a*) the Cholesky-log, and (*b*) the SSR decompositions. For the corresponding animations, see supplementary movie 6. Both simulations use the Oldroyd-B model along with the Navier-Stokes equations. Analogous results for the Stokes equations are shown in figure 1 of the main text.

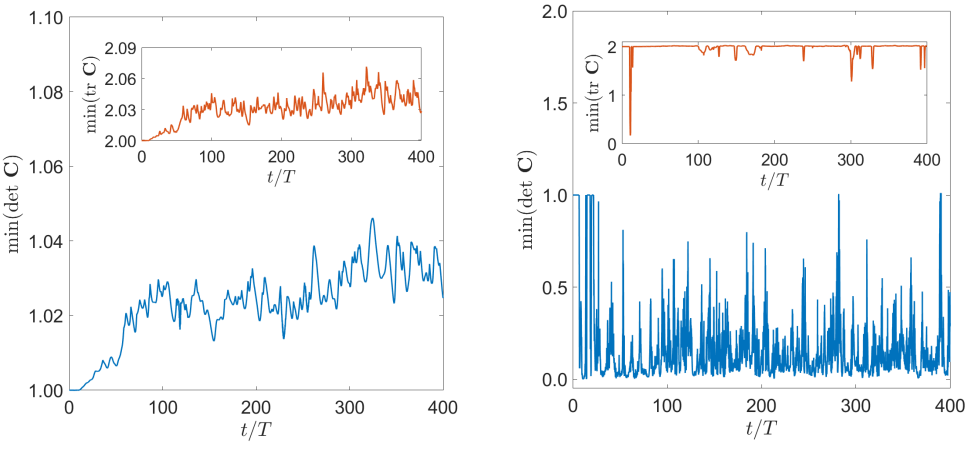

(*a*) (*b*)

FIG. 2: Time series of the minimum of det $\boldsymbol{C}$ over the domain for (*a*) the Cholesky-log, and (*b*) the SSR decompositions. The bound det $\boldsymbol{C} \geqslant 1$ is satisfied by the former simulation but is repeatedly and strongly violated by the latter. The insets show the corresponding time series of tr $\boldsymbol{C}$ which must remain greater than two. All plots refer to simulations of the Oldroyd-B model along with the Navier-Stokes equations. Analogous results for the Stokes equations are shown in figure 4 of the main text.

corresponding animations are available in supplementary movie 6). The qualitative differences that are observed in the Stokes limit (figure 1 of the main text) are seen here to persist even when the fluid inertia is nonzero (though small enough to preclude inertial instabilities). Indeed, the polymer extension field retains the spatial structure of the cellular forcing more faithfully in the Cholesky-log simulation than in the SSR simulation—the vortical cells in the latter get significantly distorted, shrinking and enlarging from time to time.

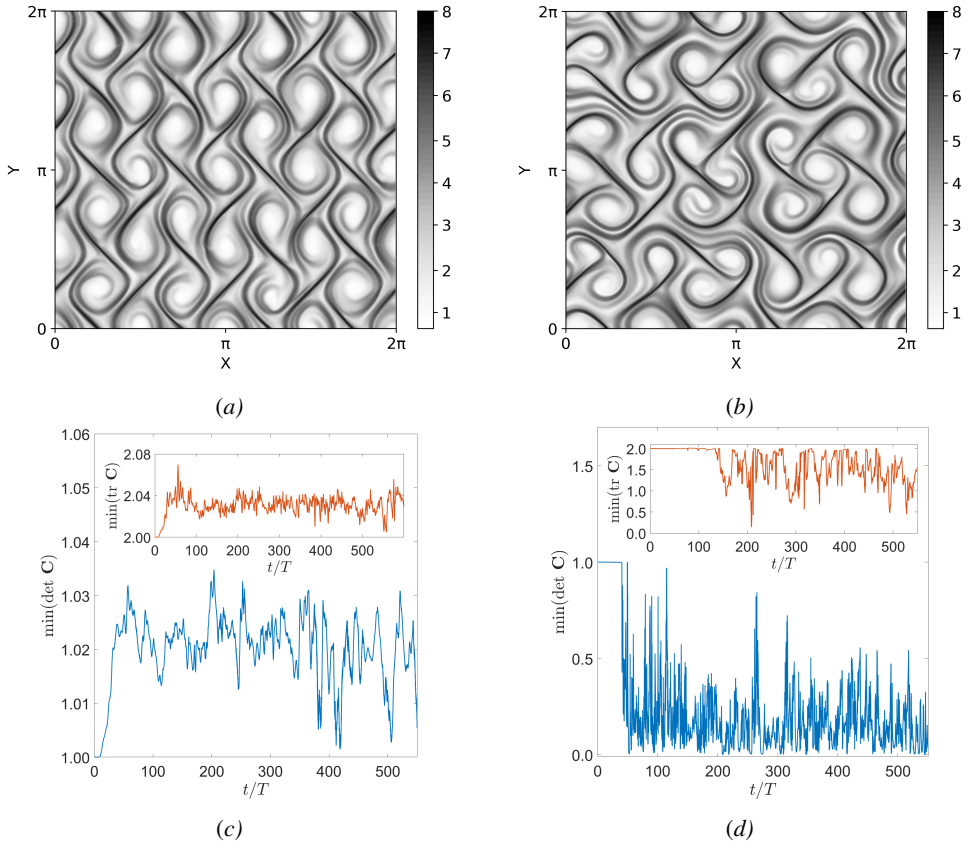

FIG. 3: Representative snapshots (instantaneous) of the logarithm of tr $\boldsymbol{C}$ for (*a*) the Cholesky-log, and (*b*) the SSR decompositions. Time series of the minimum of det $\boldsymbol{C}$ over the domain for (*c*) the Cholesky-log, and (*d*) the SSR decompositions. Both simulations use the Stokes equations and the Oldroyd-B model with a forcing wavenumber of $K = 4$. These plots are analogous to those produced with a forcing wavenumber of $K = 2$ and presented in the main text as figures 1 and 4.

The mathematical bound of Hu & Lelièvre (2007) holds for any incompressible velocity field, irrespective of whether the motion of the fluid is given by the Stokes or the Navier–Stokes equations. It can therefore be used again to discriminate between the two reformulations. We find that, similar to what is observed in the Stokes limit (figure 4 of the main text), the lower bound on det $\boldsymbol{C}$ is frequently violated in the SSR simulation, whereas it is preserved in the Cholesky-log decomposition (figure 2).

Therefore, for the same parameters and space-time resolution, the SSR reformulation is less accurate than the Cholesky-log reformulation, even when the calculations account for non-zero fluid inertia. This is unsurprising since the literature has clearly shown that the difficulties encountered in the simulation of viscoelastic flows are associated with the advection term in the constitutive equation (Vaithianathan & Collins 2003; Alves *et al.* 2021).

2. Simulations with a higher level of periodicity

Throughout the main text, the wavenumber of the periodic forcing was set at $K = 2$. We now double the forcing wavenumber to $K = 4$, thereby quadrupling the number of vortical cells, in

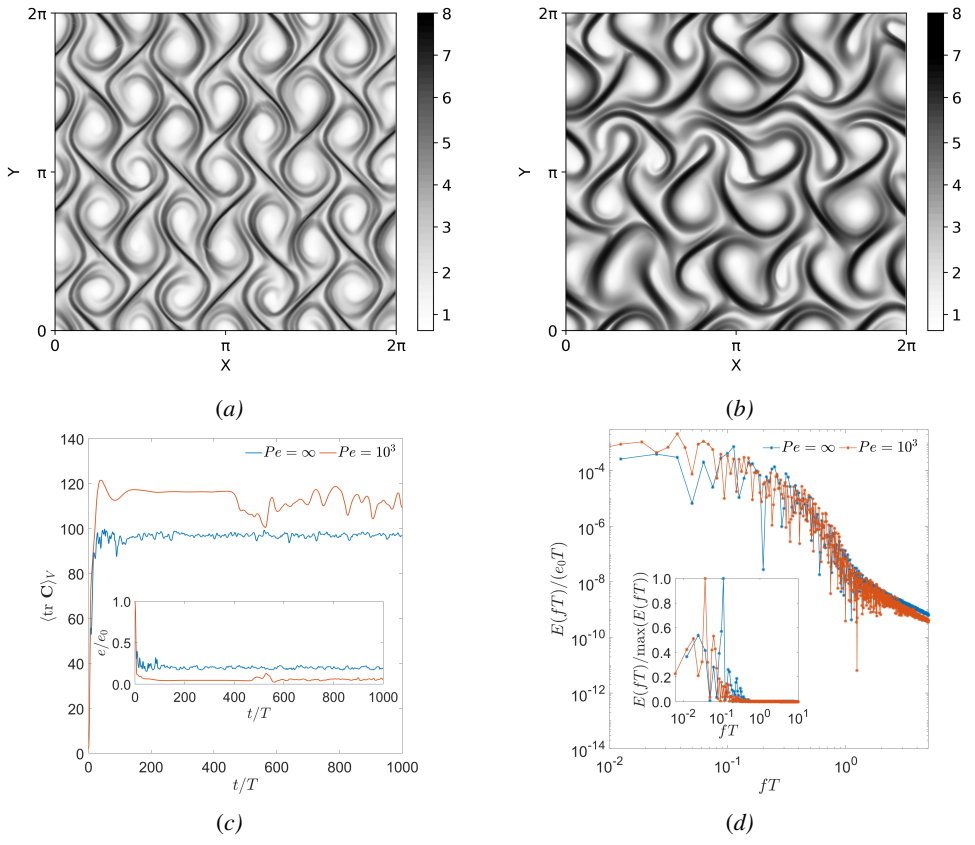

FIG. 4: Representative snapshots (instantaneous) of the logarithm of tr $\boldsymbol{C}$ for simulations without and with local artificial stress diffusion: (*a*) $Pe = \infty$ and (*b*) $Pe = 10^3$. (*c*) Time series of the space averages of tr $\boldsymbol{C}$ (main panel) and kinetic energy scaled by its Newtonian value $e(t)/e_0$ (inset). (*d*) Power spectra of the kinetic-energy fluctuations (the inset shows a semi-log plot of the normalized spectra). Both simulations use the Cholesky-log reformulation of the Oldroyd-B model along with the Stokes equation and apply a forcing wavenumber of $K = 4$. These plots are similar to those produced with a forcing wavenumber of $K = 2$ (using the FENE-P model), presented in the main text as figures 6 and 7(*b*-*c*).

order to ensure that the differences between the various simulation methods are not simply a consequence of having too small a periodic domain (relative to the forcing wavelength). Such a check is particularly important for elastic turbulence, given the results of Dzanic *et al.* (2022), who show that chaotic fluctuations are suppressed when one uses a periodic four-roll mill forcing with just four rolls (corresponding to a forcing wavelength that equals the size of the domain). Increasing the number of rolls, even by just a factor of two, allows chaotic fluctuations to develop. With this in mind, we have used a forcing wavelength that is half the domain size in the main text; below, we present results based on a further halving of the forcing wavelength and find that all our conclusions remain unchanged.

The $K = 4$ simulations produce vortical cells with half the length scale of the $K = 2$ simulations, i.e., the large length scale ℓ is halved. The large turnover time-scale T, however, is kept the same by doubling the forcing amplitude f_0 (see § 2.3 of the main text). The value of Wi is also unchanged. Thus, the $K = 4$ simulation is equivalent to doubling the domain size while maintaining $K = 2$.

Naturally, then, the $K = 4$ simulation requires twice the resolution of the $K = 2$ simulation (512^2 rather than 256^2).

Figure 3 compares the results of the Cholesky-log and SSR decompositions. Just as in the main text, we see that the vortical cells are more distorted in the SSR case (panels 3*a*-*b*), which reveals its erroneous nature by violating the lower bound on $\det \boldsymbol{C}$ (panels 3*c*-*d*). Thus, our conclusions regarding the relative accuracy of the Cholesky-log method are not affected by the level of periodicity; indeed, the results of figure 3 are analogous to that of the corresponding figures in the main text, namely figures 1 and 4.

The artifacts introduced by local artificial diffusion also remain the same with $K = 4$ as seen in figure 4. The simulation with local artificial diffusion ($Pe = 10^3$) has a distorted vortex pattern (panels 4*a*-*b*) and its temporal dynamics exhibits much larger and slower oscillations (panels 4*c*-*d*). This figure is similar to figures 6 and 7(*b*-*c*) of the main text which present the same panels for $K = 2$. The temporal kinetic-energy spectra for the $K = 4$ case (figure 4*d*) shows some quantitative differences in comparison with the $K = 2$ case (figure 7*c* of the main text), especially for the high frequencies, because while the $K = 2$ case used the FENE-P model the more computationally-demanding $K = 4$ case was run with the Oldroyd-B model. Nonetheless, in both cases, we see that the simulation with local artificial diffusion has lower (higher) energy in the moderate-to-high (low) frequencies, implying the presence of slower oscillations, which is evident in both figure 4*c* and figure 7*b* (of the main text).

3. Visualization of the vorticity field

The spatial structure of the field of vorticity is closely correlated to that of $\mathrm{tr}\,\boldsymbol{C}$, and so we have used only visualizations of $\mathrm{tr}\,\boldsymbol{C}$ in the main text to compare the structure of the vortical cells in various simulations. The qualitative differences in the large-scale flow structures that were noted in the main text are also apparent when one compares the vorticity fields. Figure 5 compares the results of simulations using the Cholesky-log and SSR decompositions. The instantaneous snapshots of the vorticity fields (panels 5*a*-*b*) reveal relatively distorted cells in the SSR simulation, in agreement with the corresponding plots of $\mathrm{tr}\,\boldsymbol{C}$ in figure 1 of the main text. The time-averaged fields (panels 5*c*-*d*) exhibit significant smearing of cell boundaries in the case of the SSR simulation, in agreement with the time-averaged fields of $\mathrm{tr}\,\boldsymbol{C}$ presented in figure 2 of the main text.

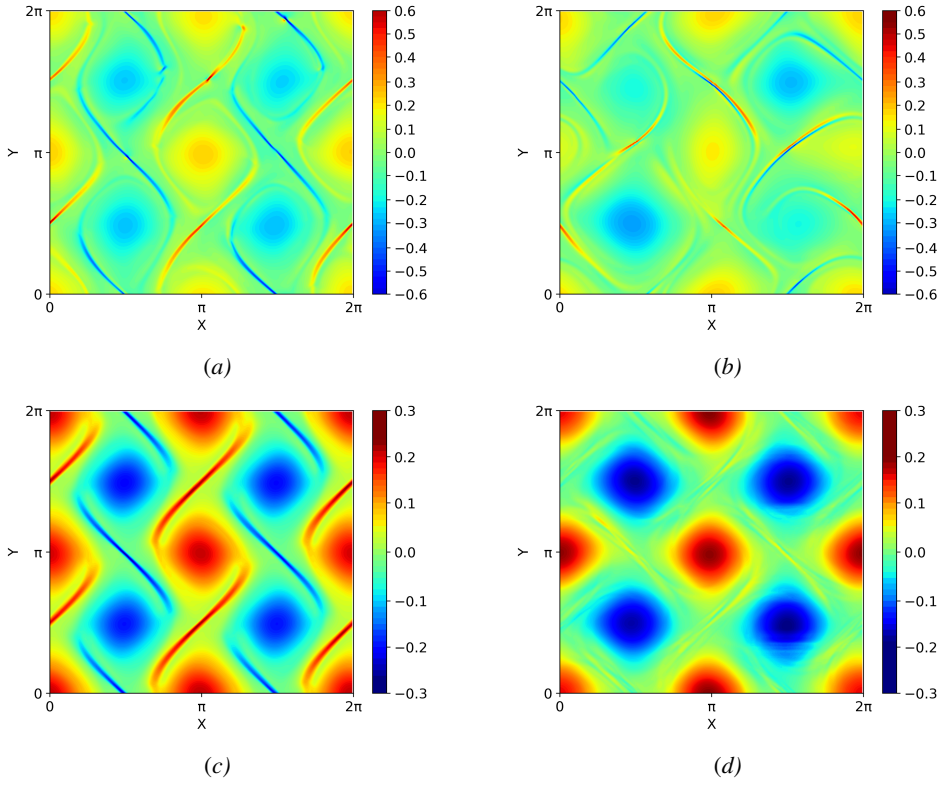

FIG. 5: Representative snapshots (instantaneous) of the vorticity field for (*a*) the Cholesky-log, and (*b*) the SSR decompositions. The corresponding time-averaged fields are presented in panels *(c)* and *(d)*. Both simulations use the Stokes equations and the Oldroyd-B model. The corresponding plots of tr $\boldsymbol{C}$ are presented in figures 1 and 2 of the main text; they reveal the same qualitative differences in the structure of the large-scale vortical cells.

References

Alves, M. A., Oliveira, P. J. & Pinho, F. T. 2021 Numerical methods for viscoelastic fluid flows. *Annu. Rev. Fluid Mech.* **53**, 509–541.

Dzanic, V., From, C.S. & Sauret, E. 2022 The effect of periodicity in the elastic turbulence regime. *J. Fluid Mech.* **937**, A31.

Gotoh, K. & Yamada, M. 1984 Instability of a cellular flow. *J. Phys. Soc. Japan* **53**, 3395–3398.

Hu, D. & Lelièvre, T. 2007 New entropy estimates for Oldroyd-B and related models. *Commun. Math. Sci.* **5**, 909–916.

Kurganov, A. & Tadmor, E. 2000 New high-resolution central schemes for nonlinear conservation laws and convection–diffusion equations. *J. Comp. Phys.* **160**, 241–282.

Vaithianathan, T. & Collins, L. R. 2003 Numerical approach to simulating turbulent flow of a viscoelastic polymer solution. *J. Comp. Phys.* **187**, 1–21.